Changing skewness of the rain distribution with warming, with and without self-aggregation

Benjamin Fildier, W D Collins, C Muller

Changing skewness of the rain distribution with warming, with and without self-aggregation

B. Fildier[1], W. D. Collins[2,3], C. Muller[1]

[1]Laboratoire de MÃľtÃľorologie Dynamique, Ãľcole Normale SupÃľrieure, Paris, France

[2]University of California, Berkeley, California, USA

[2]Lawrence Berkeley National Laboratory, Berkeley, California, USA

Key Points:

- In aggregated RCE, the mean rain fall rate is larger, but its relative increase with warming is similar to that of disorganized RCE
- Rainrates are sensitive to the strength of aggregation and are enhanced when aggregation feedbacks are combined
- In the presence of aggregation, extreme rain can increase faster than Clausius-Clapeyron because of increasing precipitation efficiency

Corresponding author: Benjamin Fildier, bfildier.work@gmail.com

Abstract

We investigate how mesoscale circulations associated with convective aggregation can modulate the sensitivity of the hydrologic cycle to warming. We quantify changes in the full distribution of rain across radiative-convective equilibrium states in a cloud-resolving model. For a given SST, the shift in mean rainfall between disorganized and organized states is associated with a shift in atmospheric radiative cooling, and is analogous to the effect of a 4K SST increase. With rising temperatures, the increase in mean rain rate is insensitive to the presence of organization, while extremes intensify faster in the aggregated state, leading to a faster amplification in the skewness of rain.

Overall, heavy rain is enhanced by 20-30% when convection aggregates, and its sensitivity to warming shows an excess of 2.5%/K beyond the Clausius-Clapeyron scaling. However, nonlinear behaviors are observed under aggregation. First, radiative- and surface-flux aggregation feedbacks have multiplicative effects on extremes, illustrating a non-trivial sensitivity to the degree of organization. Second, alternating super- and sub-Clausius-Clapeyron regimes in extreme rainfall are found as a function of SST, corresponding to varying contributions in the thermodynamic, dynamic, and precipitation efficiency increases in different SST ranges.

The potential for mesoscale circulations in amplifying the hydrologic cycle is established. However these nonlinear distortions question the quantitative relevance of idealized self-aggregation. This calls for a systematic investigation of universal relationships which capture the coupling between global energetics, aggregation feedbacks and local convection, and which could hold across domain configurations, surface boundary conditions, microphysics and turbulence schemes.

Plain Language Summary

Convective aggregation, or organization, is known to affect the spatial distribution of clouds, the wind circulation and the intensity of rain as a result of feedbacks that couple convective processes, radiative transfer in the atmosphere and energy fluxes from the Earth's surface. We investigate how the hydrologic cycle responds to warming in various conditions of forcing and aggregation feedbacks in a hierarchy of idealized simulations, and provide a fine characterization of the statistical distribution of rain in order to connect its modes of change to the physical drivers involved in aggregation. The complex behav-

ior of the rain distribution in these simulations feeds a discussion on the use of idealized experiments to investigate convective organization and on their relevance to understand future changes in the hydrologic cycle.

1 Introduction

The strength of the global hydrologic cycle can be compactly summarized by the global statistical distribution of rain. The properties of this distribution emerge from the interplay between a variety of atmospheric processes, from the large-scale energy budget and atmospheric general circulation to short convective processes. Its skewness, or "unevenness", is related to the relative importance between dry areas, drizzle and more active regimes of convection [*Pendergrass and Knutti*, 2018]. As the climate warms, the breadth of the distribution is stretched further by the tiered increases in mean and extreme precipitation [*Pendergrass and Hartmann*, 2014a], driven respectively by large-scale changes in atmospheric radiative cooling and the shorter-scale response of convection to atmospheric moistening (and in particular the Clausius-Clapeyron formula) [*Allen and Ingram*, 2002]. Emulating the relevant atmospheric radiative and convective processes with simple scaling approximations has enabled linking specific processes to the statistical properties of rain and their change with warming [*O'Gorman and Schneider*, 2009; *Pfahl et al.*, 2017; *Fildier et al.*, 2018], identifying sources of uncertainty in climate models [*O'Gorman and Schneider*, 2009; *Fildier and Collins*, 2015] and comparing the behavior of different modeling strategies [*Fildier*, 2019]. In particular, one common deficiency to all modeling frameworks is the scale separation between the large-scale circulation and small-scale convective processes due to limitations in computing capabilities. The resulting inability of models to represent the full continuum of scales responsible for the spatial organization of convection raises the central question motivating this work: as the climate warms, how could changes in the mesoscale circulations involved in the spatial structure of rain affect its global statistics?

Warmer air holds more water vapor, and that tends to cause an increase in extreme precipitation intensities at the 6-7%/K rate of the Clausius-Clapeyron (CC) formula [*O'Gorman and Muller*, 2010]. Departures from this thermodynamic reference has been noted when convection is parameterized in climate models [*Pall et al.*, 2006; *O'Gorman and Schneider*, 2009; *Fildier et al.*, 2017], as well as on short time scales for regional extremes with respect to local temperatures [*Lenderink et al.*, 2017; *Loriaux et al.*, 2013]. However, in cases of radiative-convective equilibrium (RCE, when atmospheric radiative cooling is fully balanced by latent convective heating in the absence of lateral inflow or outflow), the CC-scaling seems to hold consistently at the convective scale with respect to global temperature [*Muller et al.*, 2011; *Romps*, 2011; *Fildier et al.*, 2017; *Muller and Takayabu*,

2020]. In the latter case, mesoscale circulations are unresolved, since the simulated convection is either in a disorganized state (random, or pop-up convection) or superparameterized [*Khairoutdinov and Randall*, 2001; *Grabowski*, 2001]. Hence the question of the effects of mesoscale circulations on extreme rainfall in a changing climate remains open.

The approach chosen here is to use a cloud-resolving model (CRM) in a mesoscale RCE domain that exhibits spatial organization in the form of convective self-aggregation (see, e.g., *Wing et al.* [2017] for a review). This idealized setup is a specific case of organization, since convective organization can also encompass more general features observed such as mesoscale convective systems [*Maddox*, 1980] or patterns of shallow convection [*Feingold et al.*, 2010; *Bony et al.*, 2020]. More generally, organization can also occur in GCMs [*Coppin and Bony*, 2015], with or without convective parameterization, and under various conditions of forcing [*Wing et al.*, 2017]. Under homogeneous boundary conditions, convection can also organize in squall lines due to imposed wind shear [*Muller*, 2013]. Although changing the degree of organization (squall lines in that study) can lead to up to a doubling of extreme rainfall rates, for a given degree of organization the intensification of precipitation extremes with warming remains similar to the Clausius-Clapeyron theoretical expectation, close to about 7%/K with warming. Here instead, we will focus on the amplification of precipitation extremes when convection spontaneously self-aggregates, without any large-scale forcing or shear. In this modeling setup, a mesoscale circulation spontaneously develops within the RCE domain, and this circulation is explicitely coupled to the resolved convective processes.

Here, the internal circulations of interest emerge spontaneously in response to internal feedbacks which drive and maintain the system into a lower energy state [*Emanuel et al.*, 2014]. Self-aggregation feedbacks involve, in particular, the spatial heterogeneities in longwave radiative fluxes [*Muller and Held*, 2012] and wind-induced evaporation [*Bretherton et al.*, 2005]. In this case, it takes the form of a moist patch where convection is active, surrounded by a much drier region which lets the system lose more energy radiatively to space. This organized RCE state corresponds to different mean climate properties and climate sensitivity than the disorganized RCE state [*Mauritsen and Stevens*, 2015], as well as heterogeneous thermodynamic properties that could have substantial effects on the characteristics of the hydrologic cycle [*Tobin et al.*, 2013; *Tan et al.*, 2015].

The potential role of self-aggregation on precipitation extremes in the framework of RCE has been highlighted by several studies. At the coarse resolutions of GCMs, *Pendergrass et al.* [2016] show that precipitation extremes could increase faster with warming than the CC rate because of a changing degree of organization, and because aggregation may be more likely to occur above a critical SST threshold [*Held et al.*, 1993; *Emanuel et al.*, 2014; *Wing and Emanuel*, 2014]. *Bao et al.* [2017] further confirmed this diagnostic by showing that the ratio of extreme-rainfall-increase to mean-rainfall-increases is greater for larger degrees of organization. However, using an idealized CRM and fixed SST, *Bao and Sherwood* [2018] noticed that the statistical distribution of instantaneous precipitation does not change with the degree of aggregation because increases in precipitation efficiency are compensated by a reduced updraft speed of condensing parcels. This behavior appears independent from the microphysics scheme chosen in their study. These apparent contradictions raise the question: can self-aggregation lead to stronger mean and extreme precipitation, and can it amplify their increase with global warming?

We perform a series of CRM simulations in radiative-convective equilibrium (RCE) with fixed SSTs between 300 K and 308 K. Following most earlier studies of self-aggregation, for simplicity we neglect the Earth's rotation. This is a reasonable approximation for the study of deep tropical clouds, as the Coriolis parameter is small at low latitudes. The radiative and surface-flux feedbacks are alternately turned on or off to constrain the system in organized and disorganized states, to vary the strength of aggregation, and to remove some methodological differences for more adequate comparison with previous studies. The general procedure and simulations are introduced in section 2. Section 3 quantifies the separate roles of convective organization and surface temperatures on the distribution of rain and describes the different behavior of organized and disorganized precipitation with warming. Section 4 investigates which mechanisms involved in self-aggregation affect the strength of mean and extreme rain, in particular the circulations induced and reinforced by the radiative and surface-flux feedbacks. Section 5 investigates the thermodynamic and dynamic response of extreme events themselves in order to explain their sensitivity to the circulation. Because the relevance and strengthening of convective organization in future climates is an active area of research, we discuss the sensitivity of these results to the simulation design, and argue for future investigations of how the coupling between global climate and local convection can be modulated by these mesoscale circulations (section 6).

144 ## 2 Methodology

145 ### 2.1 Numerical experiments

146 We perform a series of experiments using the System for Atmospheric Modeling
147 (SAM) version 6.10.10 [*Khairoutdinov and Randall*, 2003]. This anelastic CRM uses as
148 prognostic variables liquid and ice static energy and non-precipitating and precipitating
149 water. Outputs are saved on hourly averages. All runs analyzed use a 4km grid resolu-
150 tion and a 1024-km square domain with doubly-periodic horizontal boundary conditions.
151 The vertical grid has 64 levels with a resolution of 500m at the tropopause and 50m at
152 the surface; in the upper levels a sponge layer is added to prevent gravity wave reflection.
153 The following parameterizations are used: a 1.5-order subgrid-scale TKE closure for tur-
154 bulent processes, the native 1-moment scheme for microphysics, and the CAM3 radiation
155 scheme [*Collins et al.*, 2006]. Surface fluxes are calculated from Monin-Obukhov similar-
156 ity theory. The model is forced with a fixed solar constant of 650 W/m^2 at a 50.0° angle,
157 typical mean insolation of equatorial regions, and with uniform SSTs of 300, 302, 304 and
158 306 K. It is run to RCE before analysis.

159 The experiments performed in this paper are summarized in table 1 at each SST.
160 The reference simulations are the first two lines. The organized run $\mathcal{O}_{\text{ref}}$ has interactive
161 surface fluxes and interactive, locally-computed radiation to allow spontaneous aggrega-
162 tion due to the surface and radiative feedbacks. In the reference disorganized run $\mathcal{D}_{\text{ref}}$, the
163 radiative feedback is removed by homogenizing the radiative heating rates Q at each time
164 step in the horizontal dimensions similarly to *Muller and Held* [2012], while the surface
165 fluxes are kept interactive to allow the simulated atmosphere to reach mass and energy
166 equilibrium. Both $\mathcal{O}_{\text{ref}}$ and $\mathcal{D}_{\text{ref}}$ are initialized from a disorganized RCE state obtained on
167 a smaller square domain 128-km wide, used for spin up at each SST. Because the equi-
168 libration time scale of atmospheric humidity is about 40 days for disorganized runs and
169 80 days for organized simulations, $\mathcal{D}_{\text{ref}}$ is run for 100 days and $\mathcal{O}_{\text{ref}}$ for 150 days, and the
170 last 50 days of each run is used for analysis. Comparing $\mathcal{O}_{\text{ref}}$ and $\mathcal{D}_{\text{ref}}$ for different SSTs
171 allows us to quantify the overall effect of organization on extreme rainfall.

Table 1. Simulations run performed for SST $\in \{300, 302, 304, 306, 308\}$ K.

Name	Radiative heating rates Q	Surface fluxes $\mathcal{F}$	Expected RCE state	Duration
$\mathcal{O}_{\text{ref}}$	interactive, heterogenous	interactive, heterogenous	organized	150 days
$\mathcal{D}_{\text{ref}}$	interactive, homogenized	interactive, heterogenous	disorganized	100 days
$\mathcal{O}\left(\mathcal{F}_{\mathcal{O}_{\text{ref}}}\right)$	interactive, heterogenous	prescribed from $\mathcal{O}_{\text{ref}}$	organized	100 days
$\mathcal{O}\left(\mathcal{F}_{\mathcal{D}_{\text{ref}}}\right)$	interactive, heterogenous	prescribed from $\mathcal{D}_{\text{ref}}$	organized	100 days
$\mathcal{D}\left(Q_{\mathcal{O}_{\text{ref}}}\right)$	radiative heating profile prescribed from $\mathcal{O}_{\text{ref}}$	interactive, heterogenous	disorganized	100 days

2.2 Separate effects of aggregation: circulation-reinforcing feedbacks and mean climate shift

The additional experiments shown on Table 1 are designed to separate the distinct roles that organization can have on the strength of mean and extreme rainfall intensities: "circulation effects", associated with the horizontal heterogeneities maintained by the radiative feedback and further strengthened by the surface flux feedback, and "mean-climate" effects, associated with shifts in the domain-averaged atmospheric radiative cooling and surface fluxes. Indeed, convective organization is associated with the development of a large-scale circulation, with low-level divergence from dry regions and low-level convergence into moist regions [*Muller and Held*, 2012]. This large-scale circulation is believed to be driven by differential radiative heating rates between moist and dry regions [*Muller and Bony*, 2015]. Convective organization is also accompanied by enhanced domain-mean outgoing longwave radiative cooling to space [*Wing and Emanuel*, 2014], as the free troposphere dries in the subsiding environment. This entails a stronger domain-averaged radiative cooling and by energy conservation a larger domain-averaged surface enthalpy flux.

Overall, this distinction between heterogeneities and domain-averages is artificial because these elements likely interact in a nonlinear fashion. But this exercise will help to emphasize the role of the spatial heterogeneities on the strength of extremes, as well as to highlight that changes in mean climate state induced by organization mainly affect the domain-mean rainfall rather than the extremes. Figure 1 explains which pairing of exper-

iments can be used to estimate the role of these individual processes on the intensity and change in extreme rainfall. These three simulations are initialized from the end state of $\mathcal{O}_{\text{ref}}$ and run for 100 days to achieve a robust steady state.

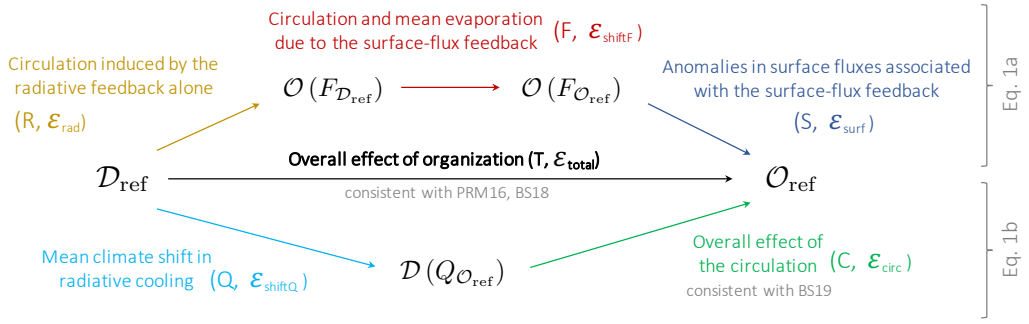

Figure 1. Summary of the experiments and their relation to individual mechanisms. The same color coding is used in later figures. Arrows are labeled with $\mathcal{E}$ symbols for defining enhancement factors (equation 1) and letters for plotting them (Figure 7).

The two pathways drawn on Figure 1 can be decomposed into a product of enhancement factors $\mathcal{E}$ for precipitation, as follows:

$$P(\mathcal{O}_{\text{ref}}) = \underbrace{\frac{P(\mathcal{O}_{\text{ref}})}{P\left(\mathcal{O}\left(\mathcal{F}_{\mathcal{O}_{\text{ref}}}\right)\right)}}_{\mathcal{E}_{\text{surf}}} \times \underbrace{\frac{P\left(\mathcal{O}\left(\mathcal{F}_{\mathcal{O}_{\text{ref}}}\right)\right)}{P\left(\mathcal{O}\left(\mathcal{F}_{\mathcal{D}_{\text{ref}}}\right)\right)}}_{\mathcal{E}_{\text{shift}\mathcal{F}}} \times \underbrace{\frac{P\left(\mathcal{O}\left(\mathcal{F}_{\mathcal{D}_{\text{ref}}}\right)\right)}{P(\mathcal{D}_{\text{ref}})}}_{\mathcal{E}_{\text{rad}}} \times P(\mathcal{D}_{\text{ref}}) \tag{1a}$$

$$\text{and} \quad P(\mathcal{O}_{\text{ref}}) = \underbrace{\frac{P(\mathcal{O}_{\text{ref}})}{P\left(\mathcal{D}\left(Q_{\mathcal{O}_{\text{ref}}}\right)\right)}}_{\mathcal{E}_{\text{circ}}} \times \underbrace{\frac{P\left(\mathcal{D}\left(Q_{\mathcal{O}_{\text{ref}}}\right)\right)}{P(\mathcal{D}_{\text{ref}})}}_{\mathcal{E}_{\text{shift}Q}} \times P(\mathcal{D}_{\text{ref}}) \tag{1b}$$

where $P(X)$ is the precipitation statistic of interest (the mean, or an extreme percentile) for simulation X. Simulations $\mathcal{O}\left(\mathcal{F}_{\mathcal{O}_{\text{ref}}}\right)$ and $\mathcal{O}\left(\mathcal{F}_{\mathcal{D}_{\text{ref}}}\right)$ use fixed sensible and latent heat fluxes, but active radiation to allow organization to persist. These prescribed surface fluxes are diagnosed from the end states of $\mathcal{O}_{\text{ref}}$ and $\mathcal{D}_{\text{ref}}$ respectively, as averages in space across the domain and in time over the last 50 days of simulation.

The comparison proceeds as follows. The organized $\mathcal{O}\left(\mathcal{F}_{\mathcal{D}_{\text{ref}}}\right)$ and the disorganized $\mathcal{D}_{\text{ref}}$ have the same mean surface fluxes, which emphasizes the role of the circulation induced by the radiative feedback alone on the intensity of extremes. The only difference between $\mathcal{O}_{\text{ref}}$ and $\mathcal{O}\left(\mathcal{F}_{\mathcal{O}_{\text{ref}}}\right)$ are the surface-flux spatial structure, so that their differences highlights how the circulation is reinforced by the spatial structure of the surface-flux feedback. Differences between $\mathcal{O}\left(\mathcal{F}_{\mathcal{O}_{\text{ref}}}\right)$ and $\mathcal{O}\left(\mathcal{F}_{\mathcal{D}_{\text{ref}}}\right)$ represents to first order the mean

shift in the atmospheric energy budget between the disorganized and organized states, which is apparent in the surface fluxes themselves in steady state.

The last simulation $\mathcal{D}\left(Q_{O_{\text{ref}}}\right)$ uses a prescribed radiative cooling profile chosen as the domain mean profile at equilibrium in the O_{ref} simulation, and interactive surface fluxes to let the system free to reach RCE. This leads to a disorganized state constrained in a similar manner as *Bao and Sherwood* [2018] and facilitates comparison with their results. By comparing $\mathcal{D}\left(Q_{O_{\text{ref}}}\right)$ with $\mathcal{D}_{\text{ref}}$, it also allows to isolate the shift in mean atmospheric radiative cooling that is induced by organization: it represents the effect of mean climate shift on precipitation intensities when convection remains disorganized, that is, without any adjustment in the circulation. Instead, differences between $\mathcal{D}\left(Q_{O_{\text{ref}}}\right)$ and O_{ref} represent the full effect of the circulation independently from changes in the mean climate.

The relationships between these simulations and their physical interpretation introduced above are summarized in Figure 2. The main effect of organization (central arrow) will be described in section 3 and the upper and lower pathways shown in the figure will be further analyzed and commented in section 4.

2.3 Methodological limitations

Figure 2 shows 2D snapshots of precipitable water PW at the end of the simulation for all simulation types and all SSTs. In some cases with fixed surface fluxes at the lowest SSTs, represented with a dashed frame on Figure 2, the system cannot maintain its aggregated states. These runs display oscillations in the spatial pattern of convection, where the convectively-active regions alternate between a small circular shapes and elongated stripes, and this behavior gradually leads to a strong drying of the entire domain (not shown). Because of the lack of robustness of the organized state, these runs will not be analyzed in this article.

3 Organized precipitation is heavier and intensifies faster with warming

3.1 Acceleration of the hydrologic cycle amplified by organization

We first investigate differences between the organized and disorganized simulations about precipitation statistics and their change with warming, using the 300K to 304K range as a reference (Figure 3).

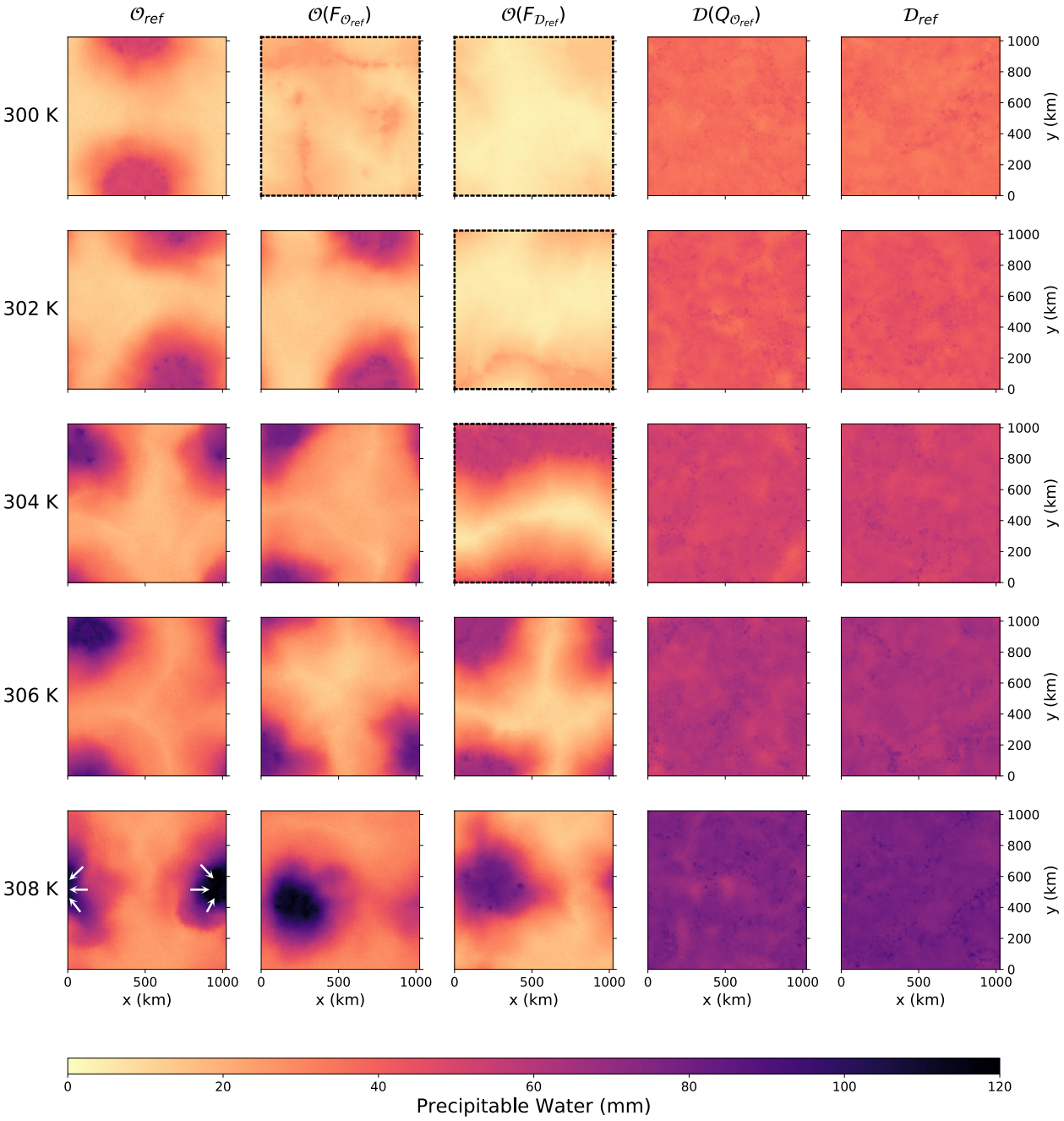

Figure 2. Snapshots of precipitable water for all SSTs (rows) and all simulation types (columns) at the end of the simulation. Simulation details are provided in Table 1. Arrows are hand-drawn on one of the simulations to indicate the direction of the low-level circulation. Simulations shown in dashed frames are discarded from the analysis because their final states do not stay robustly aggregated.

3.1.1 Simultaneous characterization of mean and extreme rainfall

Characteristics of the hydrologic cycle are quantified by calculating the full distribution of rainfall intensities and rainfall amounts. Rainfall intensities, or percentiles, are expressed in kg/m^2/s or mm/day and are calculated on hourly time scales at each percentile of the distribution of rain, including wet and dry points. Percentiles P^Q are chosen on an inverse-logarithmic scale (...,90th,99th,99.9th,...) with 10 bins regularly spaced per decade, to zoom on the extremes. This metric is traditionally used as a way to quantify extreme precipitation [*Pall et al.*, 2006; *Muller and O'Gorman*, 2011; *Fildier et al.*, 2018] that facilitates interpreting rain intensities in terms of return times or frequencies of occurrence (...,$^1/_{10}$,,$^1/_{100}$,$^1/_{1000}$,...). The second metric is rainfall exceedance amount $\overline{P}^Q$, also used by *Pendergrass and Knutti* [2018]: it has the same units as P^Q and is calculated by summing the rainfall intensities above each percentile rank Q:

$$\overline{P}^Q \equiv \int_Q^1 P^{Q'} f(Q') dQ' \tag{2}$$

where $f(Q)$ is the frequency of points in the Q^{th} percentile bin. This integrated approach enables a more comprehensive characterization of the hydrologic cycle by quantifying mean and extreme rainfall simultaneously. At the lowest percentiles, $\overline{P}^0$ corresponds to the domain mean rainfall and is controlled by the domain mean atmospheric energy budget, while at the largest percentiles with $Q \to 1$, $\overline{P}^Q$ is the mean water falling inside the most intense events that are controlled by convective processes. As a result, $\overline{P}^Q/\overline{P}^0$ represents the fraction of global rain which falls in the form of extremes.

The distributions of exceedance amounts $\overline{P}^Q$ (Figure 3a) reveal several general features of the changes in the hydrologic cycle induced by convective organization and SSTs. Two modes of change in the distribution of rain can be observed on these curves (with a similar physical interpretation as *Pendergrass and Hartmann* [2014a], although the statistical representation differs). First, a horizontal shift of $\overline{P}^Q$ towards the right (higher percentile rank Q) shows that rain becomes more extreme, meaning that given amounts of rain fall within fewer precipitation events. Second, a vertical shift of $\overline{P}^Q$ at fixed Q is characteristic of the increase in domain-mean rainfall that is consistent with changes in the atmospheric energy budget [*Pendergrass and Hartmann*, 2014a; *Fildier and Collins*, 2015]. As shown on Figure 3a, these two shifts can either occur from changes in SSTs or in the degree of convective organization. When fractional changes in $\overline{P}^Q$ are calculated for all percentiles (Figure 3c), it also becomes apparent that convective organization could be si-

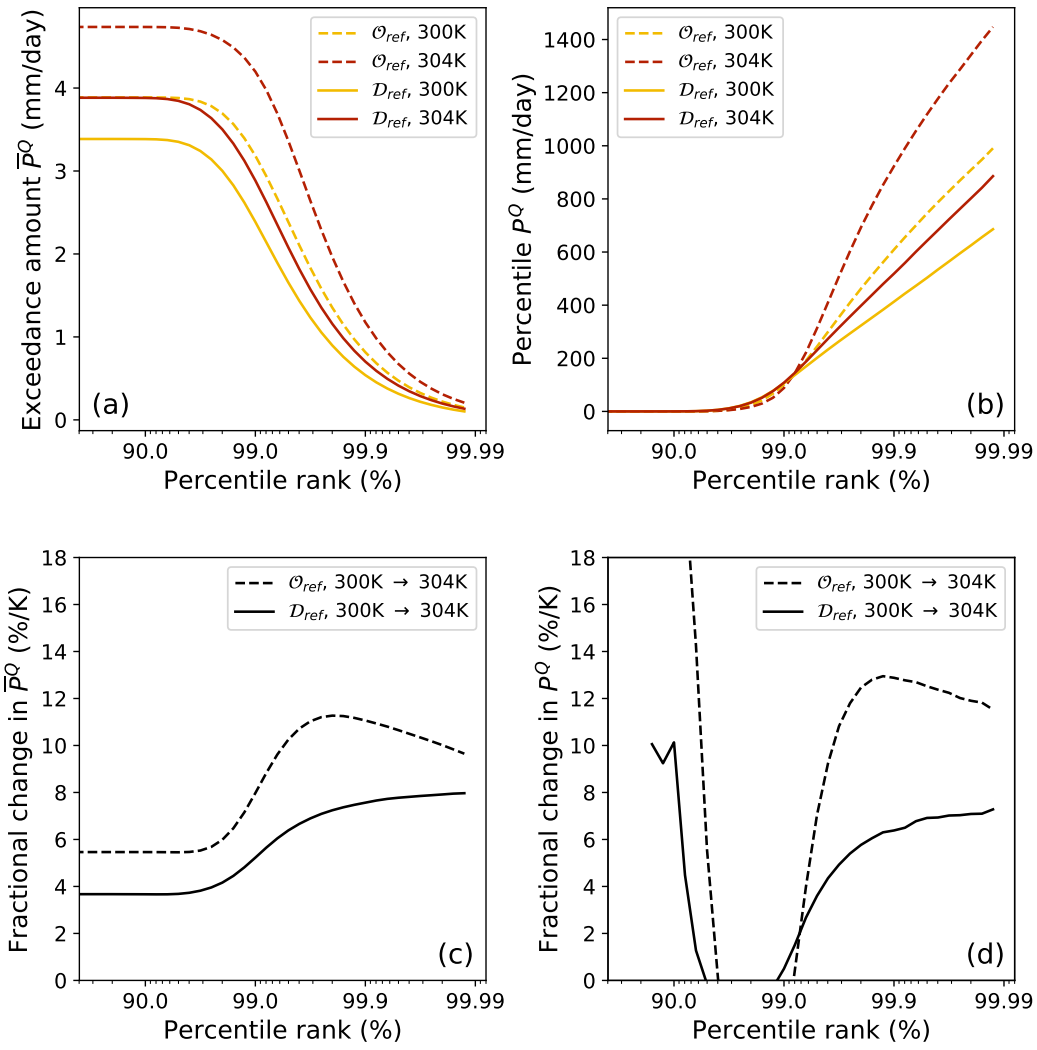

Figure 3. Comparison of statistical distribution of precipitation for the organized (solid) and disorganized (dashed) experiments at 300K (yellow) and 304K (red). The statistics are shown on individual climates (upper row) as well as their fractional changes with warming (lower row), for percentiles precipitation intensity P^Q (left panels) and exceedance amounts $\overline{P}^Q$ (right panels).

multaneously associated with larger rates of increase in domain mean rainfall (left end of the curve) and extreme rainfall (right end) as surface temperatures rise.

Focusing on the response of extreme rain intensities, it appears P^Q can be amplified by convective organization or SST (Figure 3b) and that the aggregation-driven enhancement of extremes is exacerbated with warming (Figure 3d). Note that the magnitudes of P^Q are large because they are computed on scales of 1h and 4km; 1000 mm/day approximately corresponds to 40 mm/hr, which is realistic for hourly extremes. Consistent with

the CC scaling, extreme disorganized precipitation intensities increase at about 6-7%/K, whereas organized extremes increase faster with warming, at 12.5%/K for this specific pair of SSTs (Figure 3d).

3.1.2 Apparent link between the skewness of the distribution and the degree of aggregation

The skewness of the distribution of rain, shown by the sharpness of the curves on Figure 3a, expresses the unevenness of precipitation [*Pendergrass and Knutti*, 2018]. In our simulations, it appears that this unevenness is amplified by convective organization, regardless of its effect on the mean climate.

It so happens that domain-mean rainfall rates are identical to within 0.1% in the $\mathcal{O}_{\text{ref}}^{300K}$ and $\mathcal{D}_{\text{ref}}^{304K}$ simulations (see Figure 3a) as a result of similar radiative cooling and mean surface fluxes in these two simulations. This implies that at fixed SST, the reorganization of convection induces a mean climate shift equivalent to a 4K warming for disorganized rainfall. This equivalence does not hold for extreme precipitation, as can be seen by comparing the distributions of rain intensities and exceedance amounts between $\mathcal{O}_{\text{ref}}^{300K}$ and $\mathcal{D}_{\text{ref}}^{304K}$. So, for equivalent mean climates, an organized state corresponds to a stronger skewness of the distribution of rain towards more intense extreme events. Later sections will confirm that this skewness is likely associated with differences in the circulation and in thermodynamic heterogeneities.

Following this reasoning, the enhancement of extremes by self-aggregation circulations alone can be estimated as:

$$\frac{P^{99.9}(\mathcal{O}_{\text{ref}}^{300}) - P^{99.9}(\mathcal{D}_{\text{ref}}^{300})}{P^{99.9}(\mathcal{D}_{\text{ref}}^{300})} = 46.7\% > 27.6\% = \frac{P^{99.9}(\mathcal{D}_{\text{ref}}^{304}) - P^{99.9}(\mathcal{D}_{\text{ref}}^{300})}{P^{99.9}(\mathcal{D}_{\text{ref}}^{300})} \tag{3}$$

This "4K-warming equivalence" also applies for higher SSTs: $\mathcal{O}_{\text{ref}}^{302}$ and $\mathcal{O}_{\text{ref}}^{304}$ have similar domain mean rainfall as $\mathcal{D}_{\text{ref}}^{306}$ and $\mathcal{D}_{\text{ref}}^{308}$ respectively. As a consequence, the same exercise can be done to quantify how changes in the circulation alone affect the fractional increase in extreme rainfall. Assuming that simulations $\mathcal{O}_{\text{ref}}^{T}$ and $\mathcal{D}_{\text{ref}}^{T+4K}$ have similar mean climates, the amplification of the fractional increase in extremes by the circulation alone is

$$\delta P^{99.9}(\mathcal{O}_{\text{ref}})\big|_{300\to302} - \delta P^{99.9}(\mathcal{D}_{\text{ref}})\big|_{304\to306} = 1.35\%/K \quad \text{at 300 K.} \tag{4}$$

More robust estimates of the amplification of extremes are calculated next (section 3.2), followed by a more detailed attribution of this amplification to effects to aggregation feedbacks (sections 4 and 5).

3.2 Trends in mean and extreme rain, and alternating regimes

Mean and extreme rainfall intensities are shown on Figure 4 across the complete range of SSTs. Each dot shows the value of mean and extreme rain for each simulation analyzed at each SST and the black curves represent exponential fits to the $\mathcal{O}_{\text{ref}}$ and $\mathcal{D}_{\text{ref}}$ simulations. The large offset between the two exponential fits on both graphs shows that convective organization induces a clear amplification of mean and extreme rainfall in fixed climates. This systematic effect from organization on mean rain was not always found in previous studies [*Craig and Mack*, 2013]. Mean rainfall is enhanced by a fixed fraction (≈15%) which leads to global-warming trends of similar magnitude for $\mathcal{O}_{\text{ref}}$ (3.7%) and $\mathcal{D}_{\text{ref}}$ (3.4%). Section 4 further attributes this mean rainfall enhancement to the mean climate shift induced by aggregation.

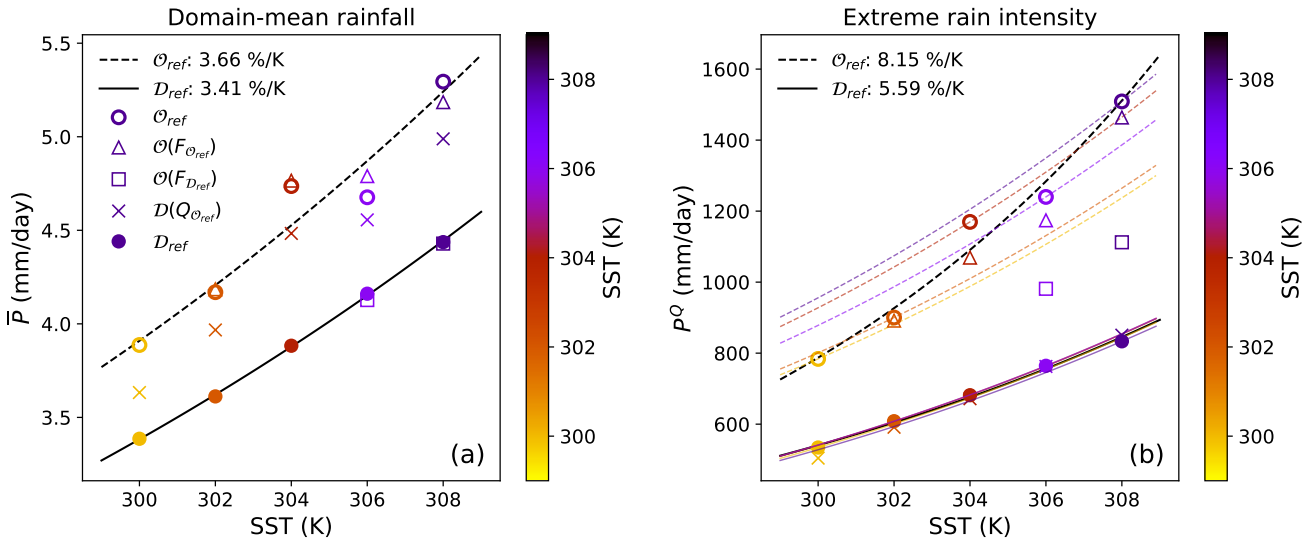

Figure 4. Strength of mean precipitation (left) and precipitation extremes $P^{99.9}$ (right) as a function of SST for all simulation types. Four simulations are excluded, as explained in section 2.2 and displayed in Figure 2. Curves show the expected Clausius-Clapeyron increase of precipitation extremes that corresponds to the reference $\mathcal{D}_{\text{ref}}$ (solid) and $\mathcal{O}_{\text{ref}}$ (dashed) simulations at each SST (color scale).

In contrast to mean precipitation, the global-warming trend of extreme rainfall intensities is accelerated in the case of convective organization, leading to super-CC rates of increase. Figure 4b shows in color the trends that would be consistent with the Clausius-Clapeyron formula, for each point (SST, P^{Q}) in the reference simulations $\mathcal{O}_{\mathrm{ref}}$ and $\mathcal{D}_{\mathrm{ref}}$. Here the trends are calculated using the Buck's formula for accuracy [*Buck A. L.*, 1981; *A. L. Buck*, 1996]:

$$P^{99.9}(T) \propto q_v^{\star}(T) \propto \exp\left(\left(18.678 - \frac{T}{234.5}\right)\frac{T}{257.14+T}\right). \tag{5}$$

For disorganized convection, the CC curves collapse onto each other, indicating a robust agreement with CC. The dashed curves, representing CC trends for organized precipitation, do not lie onto each other, indicating departures from the CC scaling. While the overall contribution of organization is a positive departure from CC of about 2.5%/K, these simulations exhibit several regimes, further detailed in section 5. Notably, super-CC increases occur below 304K and above 306K, while sub-CC increases occur in between, demonstrating a nonlinear global-warming behavior in the dynamics of extreme events due to changes in organization.

Section 4 emphasizes the multiplicity of effects that self-aggregation can have on the overall offset and trends in mean and extreme rainfall. Section 5 will investigate more specifically the reason for the overall superCC trend in extremes and the three separate regimes that appear as SST rises.

4 Shifts in mean climate and circulation strengthening

In this section we will use the intermediate simulations $\mathcal{O}\left(\mathcal{F}_{\mathcal{O}_{\mathrm{ref}}}\right)$, $\mathcal{O}\left(\mathcal{F}_{\mathcal{D}_{\mathrm{ref}}}\right)$ and $\mathcal{D}\left(\mathcal{Q}_{\mathcal{O}_{\mathrm{ref}}}\right)$ in an attempt to discuss the role of aggregation on mean and extreme rainfall via two general mechanisms, using the decomposition shown on Figure 1:

(a) *shift in the mean climate state*: changes in the atmospheric radiative cooling can be measured by comparing $\mathcal{D}_{\mathrm{ref}}$ and $\mathcal{D}\left(\mathcal{Q}_{\mathcal{O}_{\mathrm{ref}}}\right)$ (light blue arrow), and shifts in mean surface fluxes can be measured by comparing $\mathcal{O}\left(\mathcal{F}_{\mathcal{O}_{\mathrm{ref}}}\right)$ and $\mathcal{O}\left(\mathcal{F}_{\mathcal{D}_{\mathrm{ref}}}\right)$ (red arrow);

(b) *changes in the circulation* affect the local thermodynamic environment in which convective clouds can form. $\mathcal{D}\left(\mathcal{Q}_{\mathcal{O}_{\mathrm{ref}}}\right) \rightarrow \mathcal{O}_{\mathrm{ref}}$ (green) quantifies the total contribution from changes in the circulation, $\mathcal{D}_{\mathrm{ref}} \rightarrow \mathcal{O}\left(\mathcal{F}_{\mathcal{D}_{\mathrm{ref}}}\right)$ (yellow) quantifies the role of the circulation induced by the radiative feedback alone, and $\mathcal{O}\left(\mathcal{F}_{\mathcal{D}_{\mathrm{ref}}}\right) \rightarrow \mathcal{O}\left(\mathcal{F}_{\mathcal{O}_{\mathrm{ref}}}\right)$ (red) and

$O\left(\mathcal{F}_{O_{\text{ref}}}\right) \rightarrow O_{\text{ref}}$ (dark blue) both quantify the reinforcement of the circulation by the surface-flux feedback.

Interpreting each contribution separately is obviously difficult, because these mechanisms are coupled. In particular, the red arrow ($O\left(\mathcal{F}_{\mathcal{D}_{\text{ref}}}\right) \rightarrow O\left(\mathcal{F}_{O_{\text{ref}}}\right)$) can be understood as a change in the mean climate, because it corresponds to a mean increase in sensible and latent heat fluxes, but also as a change in the circulation, because surface fluxes in O_{ref} are larger in response to the stronger surface winds caused by the radiative and surface flux feedbacks. In addition, there is no unidirectional causality running from the strength of the circulation to the strength of convection, because one adjusts to changes in the other. However, this decomposition will associate changes in precipitation preferentially to shifts in mean climate or in the circulation, and will also reveal the importance of the simulation design for the distribution of rain.

We first aim at explaining the offsets between the exponential fits to $\mathcal{D}_{\text{ref}}$ and O_{ref} shown in Figures 4a and 4b. They are calculated as

$$P(\mathcal{S}) \approx \exp(\delta_{\mathcal{S}} T + \beta_{\mathcal{S}}) \tag{6}$$

where $\delta_{\mathcal{S}}$ is the overall fractional change in $P \in \{\overline{P}, P^{\text{Q}}\}$ for simulation $\mathcal{S}$. Recalling that the pathways drawn on Figure 1 can be decomposed into a product of enhancement factors $\mathcal{E}$ (Equation 1), the enhancement factor between two simulations $\mathcal{S}$ and $\mathcal{S}'$ can be written

$$\mathcal{E}_{\mathcal{S}\rightarrow\mathcal{S}'} = \exp((\delta_{\mathcal{S}'} - \delta_{\mathcal{S}})T + \beta_{\mathcal{S}'} - \beta_{\mathcal{S}}) \tag{7}$$

The enhancement factors are reported in Table 2. In the case of mean precipitation, the enhancement $\mathcal{E}$ is roughly independent of T, for its fractional change is similar in all simulations: $\delta \approx 3.5\%$/K shown on Figure 4. The mean total enhancement (the first row of the table, denoted by $\bar{P}$) is $\mathcal{E}_{\text{total}} = 1.17$, which corresponds to a 17% amplification. In the first pathway (equation (1a)), it is mostly explained by the increase in mean surface fluxes $\mathcal{E}_{\text{shift}\mathcal{F}} = 1.19$ while the two other enhancing components are negligible $\mathcal{E}_{\text{rad}} = 1.00$ and $\mathcal{E}_{\text{surf}} = 0.99$. This pathway simply highlights the consistency of a closed water budget in steady state, so that changes in mean precipitation must match changes in evaporation from the surface. In the second pathway (equation (1b)), the shift in mean radiative cooling alone cannot explain the mean rainfall shift (i.e., $\mathcal{E}_{\text{shift}Q} = 1.11$ is less than $\mathcal{E}_{\text{total}} = 1.17$), because it is partly compensated by an increase in surface sensible heat fluxes in simulation $\mathcal{D}\left(Q_{O_{\text{ref}}}\right)$ which dims the latent heat response (not shown). The

last term, corresponding to the experimental setup of previous studies [*Bao and Sherwood*, 2018], shows a complementary enhancement ($\mathcal{E}_{\text{circ}} = 1.05$). Because $\mathcal{D}\left(Q_{O_{\text{ref}}}\right)$ and O_{ref} have equal mean radiative cooling, this last term can be interpreted as the effect of the circulation on the surface enthalpy fluxes, via stronger surface winds and the drier near-surface air in the subsidence region.

Table 2. Enhancing factors $\mathcal{E}$ (see Fig. 1) to mean ($\overline{P}$) and extreme precipitation averaged between percentiles 99.9 and 99.99 (δP^{ext}), and contributions to the departures from Clausius-Clapeyron (d_{CC}):

		1st pathway (eq. 1a)			**2nd pathway (eq. 1b)**	
	$\mathcal{E}_{\text{total}}$ (T)	$\mathcal{E}_{\text{rad}}$ (R)	$\mathcal{E}_{\text{shift}\mathcal{F}}$ (F)	$\mathcal{E}_{\text{surf}}$ (S)	$\mathcal{E}_{\text{shift}Q}$ (Q)	$\mathcal{E}_{\text{circ}}$ (C)
$\overline{P}$: $\mathcal{E}$ (all SSTs)	1.17	0.99	1.19	1.00	1.11	1.05
P^{ext} : $\mathcal{E}$ (304-308K)	1.72	1.27	1.27	1.06	1.00	1.71
d_{CC}: $\delta\mathcal{E}$ (304-308K)	2.57	0.73	1.62	0.22	0.91	1.66

At fixed SST, these contributions can also be calculated for the enhancement of precipitation extremes, as shown on Figure 5a for the largest percentiles at 306 K and by the second row of Table 1 labeled P^{ext}. $\mathcal{E}_{\text{shift}Q}$ is close to 1, which suggests that for disorganized convection, changes in domain mean radiative cooling has little effect on precipitation extremes at this particular SST. It confirms recent results showing that radiative cooling mostly affects weaker rain rates [*Chua et al.*, 2019] and leaves the extremes unchanged despite the adjustment of the mean surface fluxes. As a consequence, the response of extremes to self-aggregation at fixed SST can be attributed to the overall circulation and its effect on surface fluxes: $\mathcal{E}_{\text{circ}} \approx \mathcal{E}_{\text{total}} = \frac{P^{\text{Q}}(O_{\text{ref}})}{P^{\text{Q}}(\mathcal{D}_{\text{ref}})}$. On the upper pathway, the spatial redistribution of surface enthalpy fluxes ($\mathcal{E}_{\text{surf}}$) only enhances P^{Q} by a few percent. The overall contribution is evenly split between the circulation induced by the radiative feedback and the mean effect of the surface-flux feedback: $\mathcal{E}_{\text{rad}} \approx \mathcal{E}_{\text{shift}\mathcal{F}} \approx 1.3$.

The decomposition is then applied to the super-CC rates of increase in P^{Q} (Figure 5b and the 3rd row of Table 2 labeled d_{CC}). Departures d_{CC} from the CC scaling can be decomposed as a sum of contributions coming from changes in the enhancing factors. Denoting the fractional change in precipitation extremes for a given warming gap ΔT by

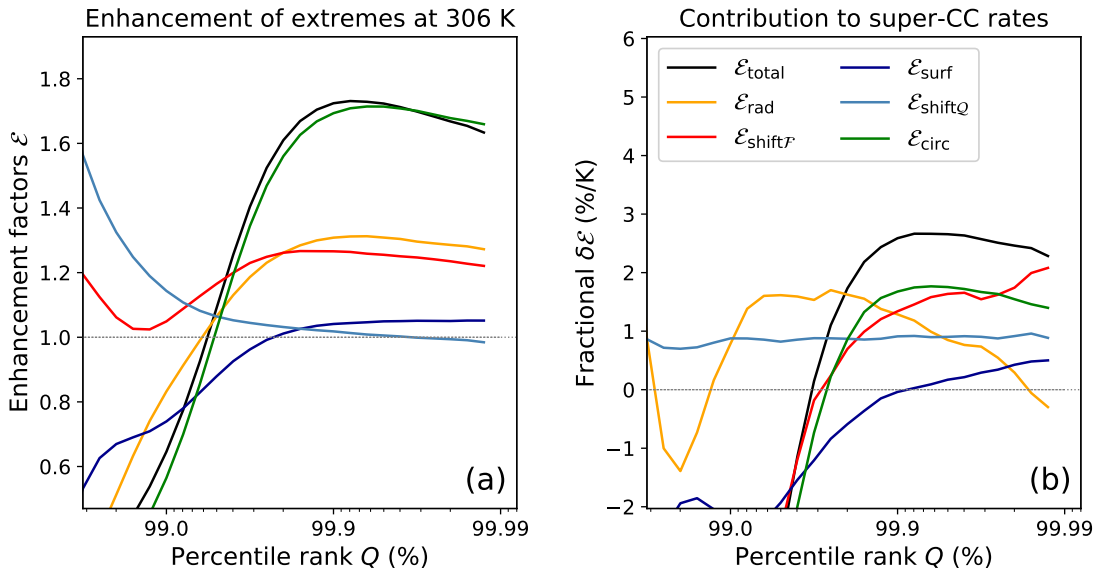

Figure 5. Enhancement of precipitation intensities P^{Q} by the circulation (green), induced by the radiative feedback (yellow), reinforced by the surface-flux feedback (dark blue and red), as well as the negligible effect of the larger radiative cooling (light blue) in a steady climate at 306K (left, multiplicative contributions); and corresponding contributions to the fractional changes δP^{Q} (right, additive contributions).

$\delta P^{\text{Q}} \equiv \Delta P^{\text{Q}}/P^{\text{Q}}/\Delta T$, departures from CC can be written as

$$\mathrm{d}_{\text{CC}} \equiv \delta P^{\text{Q}}\left(\mathcal{O}_{\text{ref}}\right) - \delta P^{\text{Q}}\left(\mathcal{D}_{\text{ref}}\right) = \delta\mathcal{E}_{\text{surf}} + \delta\mathcal{E}_{\text{shift}\mathcal{F}} + \delta\mathcal{E}_{\text{rad}} \tag{8a}$$

$$= \delta\mathcal{E}_{\text{circ}} + \delta\mathcal{E}_{\text{shift}Q}. \tag{8b}$$

where likewise $\delta\mathcal{E}_i \equiv \Delta\mathcal{E}_i/\mathcal{E}_i/\Delta T$. Each term is independent of SST and can be calculated as a difference in fractional changes for pairs of simulations: $\delta\mathcal{E}_{\mathcal{S}\to\mathcal{S}'} = \delta_{\mathcal{S}'} - \delta_{\mathcal{S}}$. Surprisingly, the increase in mean radiative cooling $\delta\mathcal{E}_{\text{shift}Q}$ does bring a small contribution of just under 1%/K to the superCC rate (0.91%/K in Table 2), despite its small role on extreme precipitation in fixed climates. This occurs because the latent heat flux increases more rapidly than the sensible flux in the $\mathcal{D}\left(Q_{\mathcal{O}_{\text{ref}}}\right)$ simulation as a function of SST, reinforcing convection (not shown). The remaining contribution comes from the overall circulation and the additional surface evaporation that it causes ($\delta\mathcal{E}_{\text{circ}} \approx 1.5$%/K). On the upper pathway, most of the change is attributable to the mean enhancement in evaporation due to the surface-flux feedback ($\delta\mathcal{E}_{\text{shift}\mathcal{F}} \approx 1.6$%/K). Changes in the radiatively-driven circulation have its strongest contribution between the 99th and 99.9th percentiles ($\delta\mathcal{E}_{\text{rad}} \approx 1.7$%/K) and affects less the heaviest rain events (≈ 0.7%/K).

Testing further the sensitivity of mean and extreme rainfall to specific self-aggregation mechanisms would likely require a more physically-based analytic framework which connects the strength of the circulation to the strength of precipitation extremes. In our case, feedback mechanisms maintain the circulation and affect the mean climate simultaneously, and their effect on rain statistics cannot be easily separated. In particular, the surface-flux feedback alone is not sufficient to maintain organization [*Holloway and Woolnough*, 2016], as seen in the $\mathcal{D}\left(Q_{O_{\text{ref}}}\right)$ experiments, so its effectiveness to strengthen the circulation cannot be physically separated from the effectiveness of the radiative feedback to organize convection in the first place.

Despite the difficulty to tease apart these contributions, two main conclusions can be drawn:

- Even for a fixed mean climate (identical values of SST, mean surface fluxes and radiative cooling), the presence of a mesoscale circulation alone can induce heavier precipitation extremes, thereby causing a stronger skewness of the distribution of rain. This result indicates that even the rarest and heaviest rain events can be understood as an integral component of the circulation. This is seen in this section by the significant enhancement $\mathcal{E}_{\text{rad}}$, although an enhancement of similar magnitude occurs in response to the stronger surface fluxes.
- The superCC trend in precipitation extremes is mainly associated with the mean enhancement of surface fluxes, indicating that the surface-flux feedback plays a major role in shaping the distribution of rain through its possible effects on convective strength. This result suggests that organized precipitation extremes could be highly sensitive to changes in the large-scale winds in the real atmosphere because of their effects on surface evaporation.

Section 5 will investigate how a reinforcement of the circulation can amplify the heaviest rain intensities.

5 The dynamics of disorganized and organized extremes

5.1 Thermodynamic, dynamic and precipitation efficiency contributions

We now seek to understand the cause for the overall super-CC trend in precipitation extremes P^{Q} across steady RCE states at different SSTs as well as the reasons for the super- and sub-CC regimes seen in section 3.2 in the O_{ref} simulation. To do so, we use

a scaling formula to approximate the largest rainfall percentiles P^{Q} from the average dynamic and thermodynamic characteristics of extreme events [*O'Gorman and Schneider*, 2009]. This expression approximates the condensation rate at each level in the troposphere as the vertical advection of saturation specific humidity $q_v^\star$ at speed w along a moist adiabat $\theta_e^\star$, and integrates it along the vertical to estimate the surface precipitation rate:

$$P^{\mathrm{Q}} \approx -\varepsilon \int_0^{z_T} w^{\mathrm{Q}} \left.\frac{\partial q_v^*}{\partial z}\right|_{\theta_e^{\star\mathrm{Q}}} \rho dz. \tag{9}$$

Superscript Q denotes that variables have been composited at the locations of extreme events: for all surface precipitation rates counted as the Qth percentile of the distribution, the profiles are sampled 1h early and averaged across rainfall events in order to reconstruct the approximate conditions in which the corresponding convective clouds were formed. The 1h time scale happens to match the characteristic timescale of convective updrafts and corresponds to the output time step. Coefficient ε can be interpreted as a proxy for the *precipitation efficiency of extremes*: as such, ε approximates the fraction of condensed water that reaches the surface, while $1-\varepsilon$ corresponds to the fraction of cloud water that mixes in the environment. ε is calculated as a tuning coefficient from a least-square fit between true percentiles P^{Q} and approximated percentiles $\int w^{\mathrm{Q}}\, \partial_z q_v^*|_{\mathrm{Q}}$ between the 99.9th and 99.99th percentile ranks. Although ε is an efficiency coefficient, it remains a tuning parameter and could potentially exceed 1. It can be affected by sampling issues and its variability can reveal a limited explanatory power of the approximation formula [*Fildier et al.*, 2018] but it also embeds additional processes such as entrainment of dry air and subtle differences in precipitation microphysics that could affect precipitation extremes [*Muller*, 2013].

This formulation facilitates decomposing the fractional changes δP^{Q} into a sum of independent contributions coming from changes in the dynamic and thermodynamic properties of extreme rainfall events. Denoting the pressure-weighted integral across the troposphere $\langle X \rangle = \int_{p_s}^{p_T} X \frac{dp}{g} \approx -\int_0^{z_T} X \rho dz$, this scaling approximation can be rewritten as

$$P^{\mathrm{Q}} \approx \varepsilon \underbrace{\langle w^{\mathrm{Q}} \rangle}_{M} \underbrace{\left\langle \frac{w^{\mathrm{Q}}}{\langle w^{\mathrm{Q}} \rangle} \left(\left.\frac{\partial q_v^*}{\partial z}\right|_{\theta_e^{\star\mathrm{Q}}} \right) \right\rangle}_{\Gamma} = \varepsilon M \Gamma \tag{10}$$

where M represents the vertically-integrated mass flux across the depth of the troposphere, such that $M/\langle 1 \rangle$ represents an effective cloud updraft velocity. In turn $\Gamma \times \langle 1 \rangle$ is a thermodynamic term representing an effective amount of moisture available for condensation, in kg/m^3.

In the case of disorganized convection, the fractional increase in extremes P^{Q} can be decomposed in a sum of fractional contributions expressed in %/K, because the terms ε, M and Γ all follow exponential increases with warming:

$$\delta P^{\mathrm{Q}} \approx \underbrace{\delta\varepsilon}_{\substack{\text{Contribution from changes in:} \\ \text{precipitation efficiency}}} + \underbrace{\delta M}_{\text{mass flux}} + \underbrace{\delta\Gamma}_{\text{thermodynamics}} \tag{11}$$

These individual contributions, precipitation efficiency ε, pressure-weighted mean vertical velocity $M/\langle 1\rangle$, in m/s, and the remaining thermodynamic term $\Gamma \times \langle 1\rangle$ which represents the moisture available for condensation in kg/m^3, are shown on Figure 6 for each SST for simulations $\mathcal{D}_{\mathrm{ref}}$ and $\mathcal{O}_{\mathrm{ref}}$.

For the reference disorganized case $\mathcal{D}_{\mathrm{ref}}$, precipitation efficiency is constant around 0.4, and the CC increase is explained by a joint and steady increase in the thermodynamic and dynamic components. Indeed, the CC increase of 5.6%/K results from an increase in the thermodynamic term Γ of +3.5%/K and increase in mass flux of +1.5%/K, while precipitation efficiency is roughly constant with warming (+0.8%/K). These numbers are consistent in relative magnitude with previous analyses of disorganized extremes [e.g. *Romps*, 2011].

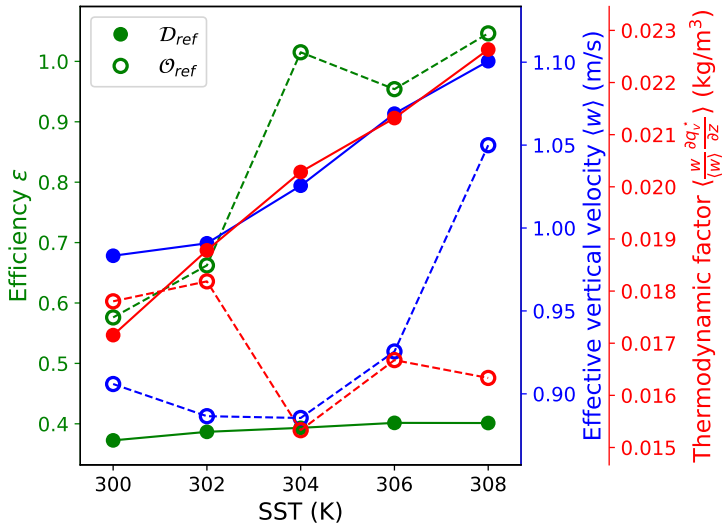

Figure 6. Precipitation efficiency (green), and the dynamic (blue) and thermodynamic (red) components of extremes rainfall P^{Q} for simulations $\mathcal{D}_{\mathrm{ref}}$ and $\mathcal{O}_{\mathrm{ref}}$.

In $\mathcal{O}_{\mathrm{ref}}$, this decomposition allows to investigate the three regimes identified in section 3.2 (superCC-subCC-superCC). The superCC rates seem to be explained by changes

in precipitation efficiency and updraft speeds. First, the large and fast increase in ε explains the first superCC regime between 300K and 304K, and it stabilizes around 1. Then, the delayed and large increase in vertical velocities at high SSTs seems to strongly contribute to the last superCC regime between 306K and 308 K. The gradual decrease in Γ and the delayed amplification of the dynamic component at higher SSTs can be related to changes in vertical velocity profiles (Figure 7b): the profile gradually shifts towards higher altitudes, causing a reduction in Γ, and vertical velocities strongly increase in the upper troposphere at high SST. This explains the simultaneous enhancement of M, but understanding what actually sets the shape of vertical velocity profiles remains an open question.

Explaining why such nonlinear dynamics occur would likely require a closer analysis of the interactions between precipitation efficiency, mixing with environmental air, and buoyancy. Although these results should be interpreted with care, it is unlikely that this behavior be an artifact of the scaling approximation: this formula closely captures the shape of the distribution tail at different SSTs, with correlation coefficients above 0.95 in all cases between the 99.9th and 99.99th percentiles, and the approximate magnitude of ε is realistic for disorganized convection [*Lutsko and Cronin*, 2018]. However, limitations of the approximation formula could lead to overestimates of precipitation efficiency, and sampling uncertainties could have caused small fluctuations in ε and the subCC increase in extremes between 304K and 306K.

5.2 Amplification of extremes by larger precipitation efficiencies

We now make a stronger case for the possible role of precipitation efficiency in amplifying the strength of extremes. Figure 7a shows the vertical profile of relative humidity at the location of precipitation extremes for the reference disorganized and organized simulations. Convective aggregation appears to bring the environmental air close to 100% relative humidity in the moist environment in which deep convective clouds form. This lower environmental saturation deficit could have a doubly enhancing effect on the surface precipitation rate: it would increase condensation, or conversion efficiency, by reducing the dilution of cloud parcels into their environment, and could increase sedimentation efficiency by reducing the re-evaporation of condensates [*Langhans et al.*, 2015; *Lutsko and Cronin*, 2018]

554 Figures 7c,d show the correspondence between the amplification in extreme pre-
555 cipitation P^{Q}, in ε and in vertically-integrated relative humidity $\langle RH \rangle$ at the location of
556 extremes, for all SSTs and all pairs of simulations as explained on Figure 1. The large
557 correlation on panel (c) confirms the importance of fluctuations in precipitation efficiency
558 for the strength of precipitation extremes. The large correlation on panel (d) suggests that
559 precipitation efficiency closely relates to the degree of saturation in the moist environment
560 where extreme events occur. This amplification is related to the strength of aggregation,
561 as this effect is more pronounced for simulations that combine several aggregation feed-
562 backs (for instance, enhancements C and R on Figures 7c,d correspond to the enhance-
563 ments $\mathcal{E}_{\text{total}}$ and $\mathcal{E}_{\text{rad}}$ respectively, introduced in section 4).

564 These results highlight the key role played by the precipitation efficiency in modu-
565 lating precipitation extremes with organization. Further investigation of the sensitivity of
566 efficiency to mesoscale organization is desirable to achieve accurate rainfall predictions in
567 a warming climate.

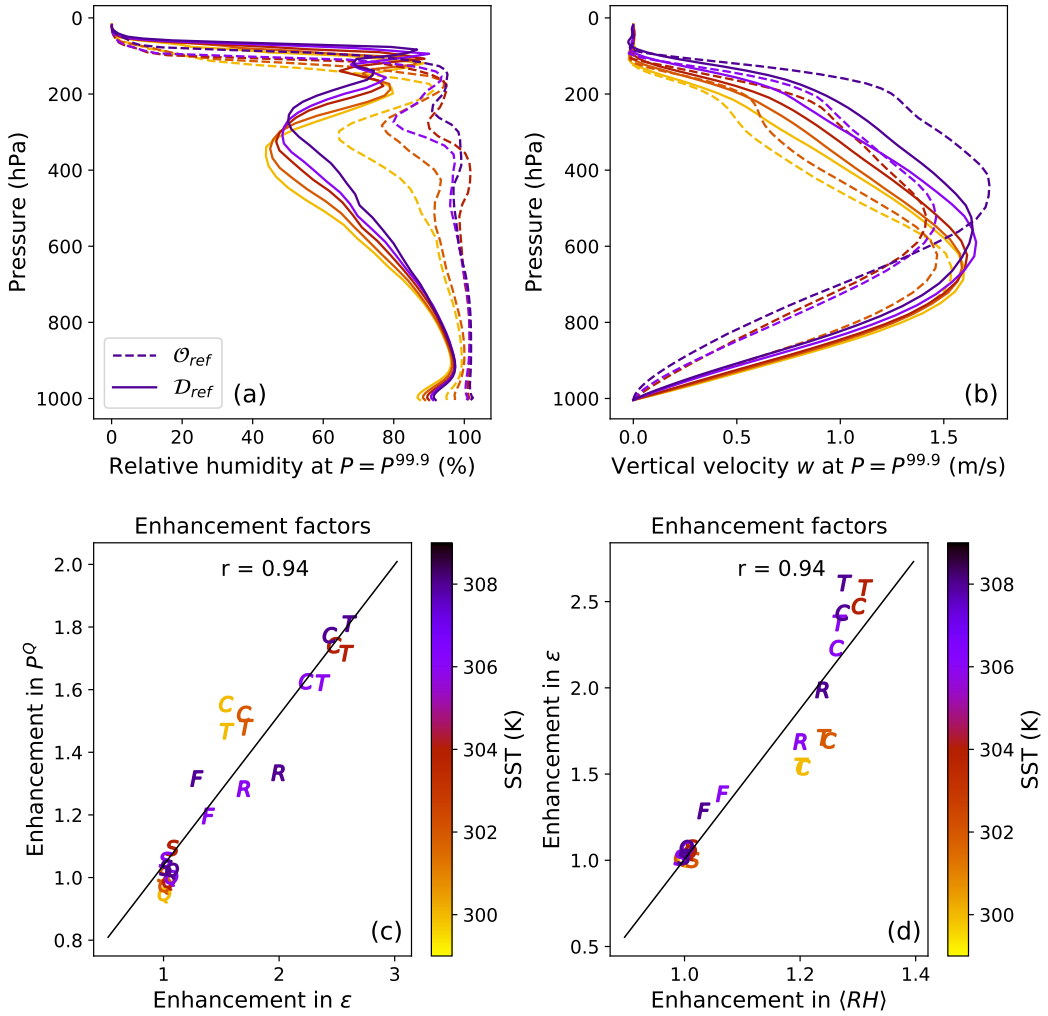

Figure 7. (a-b) Relative humidity and vertical velocity profiles at location of precipitation extremes. (c-d) Correlations between the enhancement in precipitation extremes P^Q, precipitation efficiency ε and vertically integrated relative humdity $\langle RH \rangle$ for the pairs of simulations defined in Figure 1 (letters), at all SSTs (colors).

6 Discussion

The present article summarizes the behavior of mean and extreme precipitation in conditions of disorganized and organized convection in large 3D domains. The analysis is based upon a diversity of forcing strategies and application of a large range of SSTs in order to highlight the strong sensitivity of precipitation in steady RCE states to the strength of the internal circulation and the global atmospheric energy budget. This section discusses additional lessons drawn from the variety of forcings and presents some remaining modeling simplifications that can affect the scope of these results.

6.1 Connection between mean climate, circulations and convection

Our analysis assumes that the response of mean precipitation, which is driven by the global impact of organization on the energy balance, is distinct and independent from the response of extreme precipitation, which is driven by the strength of the circulation through local changes in saturation deficit and precipitation efficiency. Even though this separation appears valid to first order, changes in mean climate properties are tightly connected to the horizontal structure of convection itself. In the case of convective aggregation, this complicates the attribution of causality and blurs the traditional distinction between the sensitivity of mean and extreme precipitation to warming.

In particular, understanding how the shape of the rainfall distribution and the intensity of rainfall extremes respond to changes in the atmospheric energy budget remains an open question. In lack of a better theory, *Pendergrass and Hartmann* [2014b] make the objective assumption that the energetic constraint on mean precipitation changes applies uniformly across all percentiles of the distribution of rain amounts. This uniformity assumption has later been disproved. *Chua et al.* [2019] show that doubling radiative cooling at fixed SST affects weak precipitation rates while leaving the heaviest rain rates unchanged. In contrast, *Thackeray et al.* [2018] show that changes in mean precipitation do correlate with changes in heavy precipitation rates across GCMs, suggesting that the strength of precipitation extremes is not actually independent from the domain-mean atmospheric radiative cooling.

In the case of disorganized convection, our simulations tend to confirm *Chua et al.* [2019]'s result because extremes are unchanged between the $\mathcal{D}_{\text{ref}}$ and $\mathcal{D}\left(\mathcal{Q}_{\mathcal{O}_{\text{ref}}}\right)$ simulations at fixed SST (Figure 4). But in the case of organized convection, changing the mean climate at fixed SST does affect the extremes, as seen by the enhancement $\mathcal{E}_{\text{shift}\mathcal{F}} > 1$ on Figure 5. In this example, both the domain-mean atmospheric radiative cooling and the circulation adjust to the increased surface fluxes, which leads to a simultaneous reinforcement of mean and extreme precipitation rates. In particular, departures from their exponential fits can be seen at the same SSTs for $\overline{P}$ and P^{Q} on Figure 4a,b.

Overall, a plausible link exists between mean and extreme rainfall in given climates, and this work suggests that the connection possibly lies in mesoscale circulation changes. As a result, these mesoscale circulations could also act as an additional degree of freedom

on their rate of change with warming as well as on the increased skewness of the rain distribution.

6.2 Sources of methodological uncertainty

Further analysis is required to test the relationships between mean/extreme precipitation and convective organization in more realistic representations of the tropical atmosphere. In particular, it seems necessary to quantify on which scales these relationships hold and validate the physical relevance of the superCC and subCC regimes identified. Indeed, several implicit methodological assumptions could bias our interpretation.

First, the limited domain size is suspected to amplify the degree of convective organization [*Cronin and Wing*, 2017], which could cause an artificial amplification of heavy precipitation intensities. On larger tropical domains than we employed, longwave radiative fluxes would tend to stretch the size of moist patches [*Beucler and Cronin*, 2019], which could damp the strong amplification in relative humidity that we find in our study. This could prevent the superCC rates that arise from increases in precipitation efficiencies, or transpose this behavior to higher SSTs. An improved characterization of the relationship between strength of self-aggregation feedbacks and domain size seems necessary to quantify the sensitivity of rain intensities to specific modeling choices.

The second issue resides in the coarse 4km resolutions used. They prevent the adequate representation of low clouds and tend to bias the system towards an excessively dry free troposphere in the subsiding regions [*Holloway et al.*, 2017]. This could lead to an overestimate of mean rainfall increases due to the model's inability to resolve the absorption of upwelling shortwave radiation reflected by stratocumulus. In addition to its role on turbulent mixing as well as rain reevaporation and cold pools [*Jeevanjee and Romps*, 2013], the coarse resolutions could bias the strength of self-aggregation feedbacks by modifying the low-level circulation induced by longwave radiative cooling in low-clouds [*Muller and Held*, 2012], thus affecting the thermodynamic environment in which extreme events occur.

Third, the timescale required for these experiments to reach equilibrium is substantially larger than the lifetime of typical MCSs [*Houze*, 2004]. Even though the effect of self-aggregation on the largest percentiles of the distribution does appear gradually during the transition between disorganized and organized states (not shown), the actual impor-

tance of aggregation for precipitation rates in shorter-lived convective systems could be smaller, and deserves further investigation.

A fourth kind of methodological limitation is the quantification of precipitation extremes themselves. In particular, the distribution of rain calculated over the entire domain actually depends on the relative occurrence of different precipitation regimes. As a result, organized RCE states over idealized small domains likely exhibit different rainfall distributions and stronger rainfall extremes than larger simulation domains with realistic occurrences of deep and shallow convective systems, even for the same conditions of forcing and in a similar mean climate.

In addition to these methodological considerations, additional uncertainties arise from the magnitude and type of forcing conditions, in addition to the choice of closure required for unresolved processes. Winds, turbulence and cloud microphysics could affect extremes indirectly through the strength of self-aggregation feedbacks and convective mixing, but also directly, by affecting convective dynamics, mixing, and condensation. *Bao and Sherwood* [2018] also report changes in precipitation efficiency with convective organization, but connect them to a microphysical response rather than changes in the local environment of convective updrafts (we note though that both can be related, as for instance changes in low-level relative humidity can affect the evaporation of rain and thus precipitation efficiency). They document changes in condensate species with a reduction in graupel production and argue that it enhances precipitation efficiency while reducing buoyancy and updraft velocity. Further analysis is desirable to test their results in SAM with two-moment microphysics schemes and under a large range of SSTs and forcing conditions.

Besides, *Lane and Moncrieff* [2015] and *Moncrieff and Lane* [2015] showed that the propagation, vertical structure and organizational properties of MCSs depend on a balance between the strength of cold pools, convective inhibition and subcloud layer saturation levels, which largely varies with large-scale wind shear conditions. Such analyses have not yet been extended to the context of self-aggregation in RCE, so that the sensitivity of self-aggregation feedbacks, precipitation efficiency and rainfall extremes to wind shear is still largely unknown.

671 ## 7 Conclusion

672 Convective organization provides a framework to study the interaction between at-
673 mospheric circulations that occur on long time scales, and convective processes that occur
674 on short time scales. Our simulations show that these mesoscale circulations can directly
675 change the spatial distribution of thermodynamic variables such as moist static energy and
676 relative humidity and affect local convective processes and the statistics of rain. The re-
677 verse interaction, namely the effect of local convective activity on the circulation strength
678 or on the redistribution of moisture [*Romps*, 2014, e.g.], is outside the scope of the present
679 study but is of importance when estimating the strengthening of organization in future cli-
680 mates.

681 This work provides evidence that a stronger degree of convective organization in
682 warmer climates can be associated with a faster increase in extreme rainfall intensities
683 than what disorganized convection indicates, with an excess relative to the Clausius-Clapeyron
684 scaling by 2.5%/K in this modeling setup. These departures correspond to variations in
685 the strength of the organization and concomitant mesoscale circulation, here simply mod-
686 ified by turning on and off the radiative and surface flux feedbacks. When convection is
687 organized, heavier extreme rainfall intensities strongly correlate with larger precipitation
688 efficiencies: this likely results from the enhanced air saturation in the moistest areas of the
689 domain and a reduced ability of cloud parcels to mix with dry air as they form.

690 Because this coupling between convection and the large-scale circulation cannot
691 be resolved on the coarse GCM grids, it could be an important source of bias for the
692 intensification of extreme rain events in current climate models. The magnitude of self-
693 aggregation feedbacks in future climates has not been quantified yet because of the sen-
694 sitivity of aggregation to model parameterizations and differences across simulation de-
695 signs. Some of the processes from which these uncertainties originate can actually affect
696 convection and precipitation directly, such as cloud microphysics and turbulent processes.
697 As a result, improved understanding of future changes in self-aggregation and precipita-
698 tion extremes could be gained simultaneously by focusing on the sensitivity of these two
699 processes to the model formulations for cloud microphysics, turbulence, surface enthalpy
700 fluxes and radiative transfer.

701 This work has demonstrated a changing behavior of precipitation extremes as a func-
702 tion of SST via multiplicative effects of self-aggregation feedbacks through a change in

the strength of aggregation. In section 6, it is proposed that the mesoscale circulations could possibly modulate the response of mean and extreme rain to global warming simultaneously. These nonlinear behaviors raise fundamental questions about the design of idealized experiments and the nature of their connection to the real atmosphere. Can these idealized model configurations (with self-aggregation and without) be interpreted quantitatively to estimate shifts in the hydrologic cycle? What correspondence can be achieved to map these results onto realistic estimates? *Tan et al.* [2015] show that a large uncertainty in current estimates of changing precipitation extremes with warming comes from lack of knowledge of how convective organization will change with warming. So, improved fundamental understanding of convective organization and its sensitivity to warming is hence an area of priority for climate model development to achieve accurate rainfall projections in a warming climate.

Acknowledgments

The authors gratefully acknowledge diverse funding agencies and resources used for this work. It was initated as part of a PhD thesis [*Fildier*, 2019] under the CASCADE project, supported by the Director, Office of Science, Office of Biological and Environmental Research of the U.S. Department of Energy under Contract No. DE-AC02-05CH11231 and DE-SC0012548. It was conducted as part of the Regional and Global Climate Modeling Program and used the computational cluster resource Cori provided by the IT Division at the Lawrence Berkeley National Laboratory. This work was later completed using funding from the European Research Council (ERC) under the European Union's Horizon 2020 research and innovation programme (Project CLUSTER, grant agreement No 805041).

The Python scripts developed for this analysis are freely available at `https://github.com/bfildier/Fildier2020`. Because of the large volume of model outputs, the simulation results are available from the authors upon request (benjamin.fildier@lmd.ens.fr) and are archived at the National Energy Research Scientific Computing Center (NERSC).

References

A. L. Buck (1996), Buck Research CR-1A User's Manual, Appendix 1, *Tech. rep.*, Buck Research Instruments, LLC.

Allen, M. R., and W. J. Ingram (2002), Constraints on future changes in climate and the hydrologic cycle, *Nature*, *419*(6903), doi:10.1038/nature01092.

Bao, J., and S. C. Sherwood (2018), The role of convective selfâĂŘaggregation in extreme instantaneous vs. daily precipitation, *Journal of Advances in Modeling Earth Systems*, p. 2018MS001503, doi:10.1029/2018MS001503.

Bao, J., S. C. Sherwood, M. Colin, and V. Dixit (2017), The Robust Relationship Between Extreme Precipitation and Convective Organization in Idealized Numerical Modeling Simulations, *Journal of Advances in Modeling Earth Systems*, *9*(6), 2291–2303, doi:10.1002/2017MS001125.

Beucler, T., and T. Cronin (2019), A budget for the size of convective self-aggregation, *Quarterly Journal of the Royal Meteorological Society*, pp. 1–20, doi:10.1002/qj.3468.

Bony, S., H. Schulz, J. Vial, and B. Stevens (2020), Sugar, Gravel, Fish, and Flowers: Dependence of Mesoscale Patterns of TradeâĂŘWind Clouds on Environmental Conditions, *Geophysical Research Letters*, *47*(7), doi:10.1029/2019gl085988.

Bretherton, C. S., P. N. Blossey, M. Khairoutdinov, C. S. Bretherton, P. N. Blossey, and M. Khairoutdinov (2005), An Energy-Balance Analysis of Deep Convective Self-Aggregation above Uniform SST, *Journal of the Atmospheric Sciences*, *62*(12), 4273–4292, doi:10.1175/JAS3614.1.

Buck A. L. (1981), New equation for computing vapor pressure and enhancement factor, *Journal of Applied Meteorology*, *20*, 1527–1532, doi:10.1175/1520-0450(1981)020<1527:NEFCVP>2.0.CO;2.

Chua, X. R., Y. Ming, and N. Jeevanjee (2019), Investigating the Fast Response of Precipitation Intensity and Boundary Layer Temperature to Atmospheric Heating Using a CloudâĂŘResolving Model, *Geophysical Research Letters*, *46*(15), 9183–9192, doi:10.1029/2019GL082408.

Collins, W. D., P. J. Rasch, B. A. Boville, J. J. Hack, J. R. McCaa, D. L. Williamson, B. P. Briegleb, C. M. Bitz, S. J. Lin, and M. Zhang (2006), The formulation and atmospheric simulation of the Community Atmosphere Model version 3 (CAM3), *Journal of Climate*, *19*(11), 2144–2161, doi:10.1175/JCLI3760.1.

Coppin, D., and S. Bony (2015), Physical mechanisms controlling the initiation of convective self-aggregation in a General Circulation Model, *Journal of Advances in Modeling Earth Systems*, *7*(4), 2060–2078, doi:10.1002/2015MS000571.

765 Craig, G. C., and J. M. Mack (2013), A coarsening model for self-organization of tropical
766 convection, *Journal of Geophysical Research Atmospheres*, *118*(16), 8761–8769, doi:
767 10.1002/jgrd.50674.

768 Cronin, T. W., and A. A. Wing (2017), Clouds, Circulation, and Climate Sensitivity in
769 a Radiative-Convective Equilibrium Channel Model, *Journal of Advances in Modeling*
770 *Earth Systems*, *9*(8), 2883–2905, doi:10.1002/2017MS001111.

771 Emanuel, K., A. A. Wing, and E. M. Vincent (2014), Radiative-convective instability,
772 *Journal of Advances in Modeling Earth Systems*, pp. 75–90, doi:10.1002/2013MS000270.

773 Feingold, G., I. Koren, H. Wang, H. Xue, and W. A. Brewer (2010), Precipitation-
774 generated oscillations in open cellular cloud fields., *Nature*, *466*(7308), 849–852, doi:
775 10.1038/nature09314.

776 Fildier, B. (2019), Physical constraints and modeling uncertainties on the acceleration of
777 the global hydrologic cycle, Ph.D. thesis.

778 Fildier, B., and W. D. Collins (2015), Origins of climate model discrepancies in atmo-
779 spheric shortwave absorption and global precipitation changes, *Geophysical Research*
780 *Letters*, *42*(20), 8749–8757, doi:10.1002/2015GL065931.

781 Fildier, B., H. Parishani, and W. D. Collins (2017), Simultaneous characterization of
782 mesoscale and convective-scale tropical rainfall extremes and their dynamical and ther-
783 modynamic modes of change, *Journal of Advances in Modeling Earth Systems*, *9*(5),
784 2103–2119, doi:10.1002/2017MS001033.

785 Fildier, B., H. Parishani, and W. D. Collins (2018), Prognostic Power of Extreme Rainfall
786 Scaling Formulas across Space and Time Scales, *Journal of Advances in Modeling Earth*
787 *Systems*, doi:10.1029/2018MS001462.

788 Grabowski, W. W. (2001), Coupling Cloud Processes with the Large-Scale Dynamics Us-
789 ing the Cloud-Resolving Convection Parameterization (CRCP), *Journal of the Atmo-*
790 *spheric Sciences*, *58*(9), 978–997, doi:10.1175/1520-0469(2001)058<0978:CCPWTL>
791 2.0.CO;2.

792 Held, I. M., R. S. Hemler, V. Ramaswamy, I. M. Held, R. S. Hemler, and V. Ramaswamy
793 (1993), Radiative-Convective Equilibrium with Explicit Two-Dimensional Moist
794 Convection, *Journal of the Atmospheric Sciences*, *50*(23), 3909–3927, doi:10.1175/
795 1520-0469(1993)050<3909:RCEWET>2.0.CO;2.

796 Holloway, C. E., and S. J. Woolnough (2016), The sensitivity of convective aggregation to
797 diabatic processes in idealized radiative-convective equilibrium simulations, *Journal of*

Advances in Modeling Earth Systems, *8*(1), 166–195, doi:10.1002/2015MS000511.

Holloway, C. E., A. A. Wing, S. Bony, C. Muller, H. Masunaga, T. S. L'Ecuyer, D. D. Turner, and P. Zuidema (2017), Observing Convective Aggregation, *Surveys in Geophysics*, *38*(6), 1199–1236, doi:10.1007/s10712-017-9419-1.

Houze, R. A., Jr. (2004), Mesoscale convective systems, *Rev. Geophys.*, *42*(4), RG4003.

Jeevanjee, N., and D. M. Romps (2013), Convective self-aggregation, cold pools, and domain size, *Geophysical Research Letters*, *40*(5), 994–998, doi:10.1002/grl.50204.

Khairoutdinov, M. F., and D. A. Randall (2001), A cloud resolving model as a cloud parameterization in the NCAR Community Climate System Model: Preliminary results, *Geophysical Research Letters*, *28*(18), 3617–3620, doi:10.1029/2001GL013552.

Khairoutdinov, M. F., and D. A. Randall (2003), Cloud Resolving Modeling of the ARM Summer 1997 IOP: Model Formulation, Results, Uncertainties, and Sensitivities, *Journal of the Atmospheric Sciences*, *60*(4), 607–625, doi:10.1175/1520-0469(2003)060<0607:CRMOTA>2.0.CO;2.

Lane, T. P., and M. W. Moncrieff (2015), Long-Lived Mesoscale Systems in a LowâĂŞConvective Inhibition Environment. Part I: Upshear Propagation, *Journal of the Atmospheric Sciences*, *72*(11), 4297–4318, doi:10.1175/jas-d-15-0073.1.

Langhans, W., K. Yeo, D. M. Romps, W. Langhans, K. Yeo, and D. M. Romps (2015), Lagrangian Investigation of the Precipitation Efficiency of Convective Clouds, *Journal of the Atmospheric Sciences*, *72*(3), 1045–1062, doi:10.1175/JAS-D-14-0159.1.

Lenderink, G., R. Barbero, J. M. Loriaux, and H. J. Fowler (2017), Super-Clausius-Clapeyron scaling of extreme hourly convective precipitation and its relation to large-scale atmospheric conditions, *Journal of Climate*, *30*(15), 6037–6052, doi:10.1175/JCLI-D-16-0808.1.

Loriaux, J. M., G. Lenderink, S. R. De Roode, A. P. Siebesma, J. M. Loriaux, G. Lenderink, S. R. D. Roode, and A. P. Siebesma (2013), Understanding Convective Extreme Precipitation Scaling Using Observations and an Entraining Plume Model, *Journal of the Atmospheric Sciences*, *70*(11), 3641–3655, doi:10.1175/JAS-D-12-0317.1.

Lutsko, N. J., and T. W. Cronin (2018), Increase in Precipitation Efficiency With Surface Warming in RadiativeâĂŘConvective Equilibrium, *Journal of Advances in Modeling Earth Systems*, *10*(11), 2992–3010, doi:10.1029/2018MS001482.

Maddox, R. A. (1980), Mesoscale Convective Complexes, *Bulletin of the American Meteorological Society*, *61*, 1374–1387, doi:10.2307/26221473.

Mauritsen, T., and B. Stevens (2015), Missing iris effect as a possible cause of muted hydrological change and high climate sensitivity in models, doi:10.1038/ngeo2414.

Moncrieff, M. W., and T. P. Lane (2015), Long-Lived Mesoscale Systems in a LowâĂŞConvective Inhibition Environment. Part II: Downshear Propagation, *Journal of the Atmospheric Sciences*, *72*(11), 4319–4336, doi:10.1175/jas-d-15-0074.1.

Muller, C. (2013), Impact of Convective Organization on the Response of Tropical Precipitation Extremes to Warming, *Journal of Climate*, *26*(14), 5028–5043, doi:10.1175/JCLI-D-12-00655.1.

Muller, C., and S. Bony (2015), What favors convective aggregation and why?, *Geophysical Research Letters*, *42*(13), 5626–5634, doi:10.1002/2015GL064260.

Muller, C. J., and I. M. Held (2012), Detailed Investigation of the Self-Aggregation of Convection in Cloud-Resolving Simulations, *Journal of the Atmospheric Sciences*, *69*(8), 2551–2565, doi:10.1175/JAS-D-11-0257.1.

Muller, C. J., and P. A. O'Gorman (2011), An energetic perspective on the regional response of precipitation to climate change, *Nature Climate Change*, *1*(5), 266–271, doi:10.1038/nclimate1169.

Muller, C. J., and Y. Takayabu (2020), Response of precipitation extremes to warming: what have we learned from theory and idealized cloud-resolving simulations, and what remains to be learned?, *Environmental Research Letters*, *15*, doi:10.1088/1748-9326/ab7130.

Muller, C. J., P. A. O'Gorman, and L. E. Back (2011), Intensification of Precipitation Extremes with Warming in a Cloud-Resolving Model, *Journal of Climate*, *24*(11), 2784–2800, doi:10.1175/2011JCLI3876.1.

O'Gorman, P., and C. Muller (2010), How closely do changes in surface and column water vapor follow clausius–clapeyron scaling in climate change simulations?, *Environ. Res. Lett.*, *5*(2), 025,207.

O'Gorman, P. A., and T. Schneider (2009), Scaling of Precipitation Extremes over a Wide Range of Climates Simulated with an Idealized GCM, *Journal of Climate*, *22*(21), 5676–5685, doi:10.1175/2009JCLI2701.1.

Pall, P., M. R. Allen, and D. A. Stone (2006), Testing the ClausiusâĂŞClapeyron Constraint on Changes in Extreme Precipitation Under CO2 Warming, *Climate Dynamics*, *28*(4), 351–363, doi:10.1007/s00382-006-0180-2.

Pendergrass, A. G., and D. L. Hartmann (2014a), The Atmospheric Energy Constraint on Global-Mean Precipitation Change, *Journal of Climate*, *27*(2), 757–768, doi:10.1175/JCLI-D-13-00163.1.

Pendergrass, A. G., and D. L. Hartmann (2014b), Two modes of change of the distribution of rain, *Journal of Climate*, p. 141006071055006, doi:10.1175/JCLI-D-14-00182.1.

Pendergrass, A. G., and R. Knutti (2018), The Uneven Nature of Daily Precipitation and Its Change, *Geophysical Research Letters*, *45*(21), 11,980–11,988, doi:10.1029/2018GL080298.

Pendergrass, A. G., K. A. Reed, and B. Medeiros (2016), The link between extreme precipitation and convective organization in a warming climate: Global radiative-convective equilibrium simulations, *Geophysical Research Letters*, *43*(21), 11,445–11,452, doi:10.1002/2016GL071285.

Pfahl, S., P. A. O'Gorman, and E. M. Fischer (2017), Understanding the regional pattern of projected future changes in extreme precipitation, *Nature Climate Change*, *7*(6), 423–428, doi:10.1038/nclimate3287.

Romps, D. M. (2011), Response of Tropical Precipitation to Global Warming, *Journal of the Atmospheric Sciences*, *68*(1), 123–138, doi:10.1175/2010JAS3542.1.

Romps, D. M. (2014), An analytical model for tropical relative humidity, *Journal of Climate*, pp. 7432–7449, doi:10.1175/JCLI-D-14-00255.1.

Tan, J., C. Jakob, W. B. Rossow, and G. Tselioudis (2015), Increases in tropical rainfall driven by changes in frequency of organized deep convection, *Nature*, *519*(7544), 451–454, doi:10.1038/nature14339.

Thackeray, C. W., A. M. DeAngelis, A. Hall, D. L. Swain, and X. Qu (2018), On the Connection Between Global Hydrologic Sensitivity and Regional Wet Extremes, *Geophysical Research Letters*, *45*(20), 11,343–11,351, doi:10.1029/2018GL079698.

Tobin, I., S. Bony, C. E. Holloway, J.-Y. Grandpeix, G. Sèze, D. Coppin, S. J. Woolnough, and R. Roca (2013), Does convective aggregation need to be represented in cumulus parameterizations?, *Journal of Advances in Modeling Earth Systems*, *5*(4), 692–703, doi:10.1002/jame.20047.

Wing, A. A., and K. A. Emanuel (2014), Physical mechanisms controlling self-aggregation of convection in idealized numerical modeling simulations, *Journal of Advances in Modeling Earth Systems*, *6*(1), 59–74, doi:10.1002/2013MS000269.

Wing, A. A., K. Emanuel, C. E. Holloway, and C. Muller (2017), Convective Self-Aggregation in Numerical Simulations: A Review, doi:10.1007/s10712-017-9408-4.